ELSEVIER

Biomaterials 22 (2001) 3105–3112

Biomaterials

www.elsevier.com/locate/biomaterials

Effect of chemical composition on hydrophobicity and zeta potential of plasma sprayed HA/CaO–P_2O_5 glass coatings

M.P. Ferraz[a], F.J. Monteiro[a,b], A.P. Serro[c], B. Saramago[c], I.R. Gibson[d], J.D. Santos[a,b,*]

[a]*Laboratório de Biomateriais, Instituto de Engenharia Biomédica (INEB), Rua do Campo Alegre 823, 4150 Porto, Portugal*
[b]*Departamento de Engenharia Metalúrgica e de Materiais, Faculdade de Engenharia, Universidade do Porto, Rua dos Bragas, 4099 Porto Codex, Portugal*
[c]*Centro de Química Estrutural, Complexo I, Instituto Superior Técnico, Av. Rovisco Pais, 1096 Lisboa, Codex, Portugal*
[d]*IRC in Biomedical Materials, Queen Mary and Westfield College, London, UK*

Received 25 September 2000; accepted 29 January 2001

Abstract

Multilayered plasma sprayed coatings on the surface of Ti–6Al–4 V alloys have been prepared, which were composed of an underlayer of HA and a surface layer of a CaO–P_2O_5 glass–HA composite, with 2 or 4 wt% of glass. Contact angle and surface tension variation with time, for both water and a protein solution, were determined by the sessile and pendent drop methods respectively using the ADSA-P software. Wettability studies showed that hydrophobicity of the coatings increase with the glass addition. The work of adhesion of albumin was also altered in a controlled manner by the addition of the CaO–P_2O_5 glass, being lower on the composite coatings than on HA. Zeta potential (*ZP*) results showed that composite coatings presented a higher net negative charge than HA coatings and that *ZP* values were also influenced by the content of the glass. This study demonstrated that the surface properties of those coatings may be modified by the addition of CaO–P_2O_5 glass. © 2001 Published by Elsevier Science Ltd.

Keywords: Hydroxyapatite glass composites; Coatings; Hydrophobicity; Surface tension zeta potential

1. Introduction

Plasma-sprayed hydroxyapatite (HA) coatings applied onto metallic substrates are currently being used as implants and prostheses in many dental and orthopaedic applications. These coated biomaterials combine high strength and fracture toughness of the metallic substrate with the bioactivity of the HA coatings. Several studies have shown that this system is more effective than Ti–6Al–4 V alloys [1–6].

Recent studies have demonstrated that multilayered coatings composed of mixtures of CaO–P_2O_5 glasses and HA may present several advantages over HA coatings alone [7,8]. In fact, HA although being bioactive presents slow osteoconduction in vivo, requiring long-term immobilisation periods after surgery. The use of multilayered coatings of HA/CaO–P_2O_5 glass composite allows for a faster Ca and P ionic exchange with the local environment after implantation, due to the high solubility induced by the CaO–P_2O_5 glass. This highly soluble phase is expected to facilitate the mineralisation process, as observed for biphasic calcium phosphates, for example. On the other hand, the presence of an underlayer of HA, which will be more stable than the CaO–P_2O_5 glass, facilitates long-term osseointegration and therefore stabilisation of the prosthesis.

Previous in vitro bioactivity testing using simulated body fluid (SBF) has shown that during the immersion of glass reinforced HA coatings, dissolution of the coating surface occurred and apatite layer formation on the surface took place faster than on purely HA coatings [8]. This is a strong indication that composite coatings induce faster mineralisation in vitro than HA coatings.

The effects of the glass reinforced HA coatings on bone cell growth and function have also been previously studied [9]. Human bone marrow cells cultured on coatings, previously immersed in α-MEM, proliferate and secrete extracellular matrix. In contrast, significant differences were found in cell behaviour in contact with non-immersed coatings, where the formation of a continuous

* Corresponding author. Laboratório de Biomateriais, Instituto de Engenharia Biomédica (INEB), Rua do Campo Alegre 823, 4150 Porto, Portugal. Tel.: + 351-22-2041789; fax: + 351-22-6094567.
E-mail address: jdsantos@fe.up.pt (J.D. Santos).

0142-9612/01/$ - see front matter
PII: S0142-9612(01)00059-X

cell layer was observed on the surface of composite coatings but not on HA coatings.

The differences in cell behaviour of bone marrow cells may reflect differences in surface characteristics. Therefore, surface properties such as surface free energy and surface charge could be critical for assessing the biological performance of composite coatings given that the formation of a protein layer adsorbed on the surface of biomaterials is the first step in the interaction process of implanted material and host biological tissues. In fact, cell attachment, spreading and function development is strongly influenced by the protein adsorption, and ultimately by surface characteristics like hydrophobicity and electric surface charge [10,11].

Contact angle measurements can be used for studies of wettablility, interfacial free energy and in situ studies of protein adsorption [12]. The pendent and sessile drop methods are the most commonly used techniques for the measurement of surface tension and contact angle, respectively.

The time dependence of wetting phenomena involving biological model fluids and the surface of coated implants has a fundamental importance in the understanding of biological process leading to osteointegration. Adsorption of blood proteins on artificial implant materials is the first step of a sequence of events that may lead to biocompatibility of the implant. Blood is the first medium encountered after surgical procedure thus governing the subsequent cell attachment, and albumin is one of the proteins present in higher percentage in the human body.

In this work, wettability and zeta potential studies were performed to characterise the hydrophobicity, surface free energy, and surface charge of glass reinforced HA coatings. For the wettability studies a solution of bovine serum albumin (BSA) in SBF was used.

2. Materials and methods

2.1. Materials preparation

A $CaO–P_2O_5$ based glass (G1), with the following chemical composition (in mol%): $35P_2O_5–35CaO–20Na_2O–10K_2O$, was prepared from reagent grade chemicals using a conventional melting technique. Glass and HA powders (P120 batch, Plasma Biotal, Tideswell, UK) were wet-mixed in methanol and a content of 2 and 4 wt% of glass was added to HA. The method used to prepare the glass reinforced HA composites has been fully described elsewhere [13]. Mixed powders were then dried, isostatically pressed at 200 MPa and sintered. Samples were then milled and sieved to provide a particle size distribution between 53 and 150 μm.

Titanium alloy samples (Ti–6Al–4 V) of 10×20 and 2 mm thick were coated using atmospheric plasma spraying employing HA and composite powders. An atmospheric plasma spraying technique was performed using a Plasma Technik automated equipment and all substrates were coated at the same time, in order to ensure the same coating thickness. Coating thickness was determined by micrometer and SEM measurements. Three types of coatings were prepared as in Table 1. Uncoated Ti–6Al–4 V substrates were used as a control in all performed tests.

Table 1
Coating composition (wt%) and thickness (μm)

Sample	Composition (wt%)		Coating thickness (μm)	
	First layer	Second layer	First layer	Second layer
HA	HA	—	120	—
HA/$G_1$2	HA	98% HA + 2% G_1	60	60
HA/$G_1$4	HA	96% HA + 4% G_1	60	60

2.2. Quantitative phase analysis

X-ray diffraction (XRD) analysis was performed on the coated samples, in a Siemens D5000 diffractometer. Using flat geometry, data were collected from 5° to 110° 2θ values, with a step size of 0.02° and a count time of 12 s/step. Quantitative phase analysis was performed by Rietveld method using General Structure Analysis Software (GSAS; Los Alamos National Laboratory). A complete description of the methodology used has been fully given previously [14].

2.3. Zeta potential measurements

For zeta potential measurements coatings were detached from the Ti–6Al–4 V substrate after plasma spraying and milled in an agate ball mill pot. Particle size distribution and zeta potential (ZP) were measured in a Brookhaven ZetaPlus instrument. Particle size was below 1.3 μm, with 90% of the particles below 1 μm. Zeta potential was calculated automatically by the ZetaPlus instrument based on Smoluchowski's equation

$$ZP = 4\pi \frac{\eta}{D} EM, \quad (1)$$

where η is the viscosity of the suspending liquid, D the dielectric constant of the suspending liquid, and EM the electrophoretic mobility. Triplicate measurements were performed for each testing material at pH 7.2 using 10^{-3} M KCl solution.

2.4. Roughness measurements

Roughness measurements were performed on coated samples using a laser rugosimeter Pertometer S3P. Arithmetical mean roughness (R_a) values were taken at three different points on each sample. For each material six samples were analysed; therefore a total of 18 areas were recorded. Measurements were performed along 1.75 mm long lines on the surface, through five times in 0.250 mm steps.

2.5. Surface tension and contact angles determination

The time evolution of the liquid surface tension was obtained from the analysis of the change in the shape of pendent drops kept inside a closed thermostatted stainless-steel chamber, whose atmosphere was saturated with a pool of the liquid sample. The drops were generated at the tip of a Teflon capillary fitted to the metallic needle of a micrometric syringe (Gilmont Instruments). The first drop was recorded as soon as stabilisation was achieved and images were taken every 10 s in the initial 60 s and every 20 s in the following 20 min. The drop image was recorded using a videocamera mounted on a microscope. The profile of the drop was analysed by the program Axisymmetric Drop Shape Analysis-Profile (ADSA-P) developed by Neumann and co-workers [15,16], consisting of the construction of an objective function which expresses the deviation of the physically observed profile of a drop from a theoretical Laplacian curve, and numerically minimises it with the liquid surface tension as one of the adjustable parameters. The measurements were carried out in 10 different drops, at room temperature (25°C) inside the above-mentioned thermostatted chamber.

Contact angles were obtained by the sessile drop method using the equipment described above, in 10 different samples. Drops were deposited with the micrometric syringe on the materials, which were inside the thermostatted chamber, previously saturated with a pool of the liquid in use. The drop was recorded as soon as stabilisation was achieved, and images were taken every 5 s in the initial 20 s, every 10 s till 60 s and every 30 s in the following time (200 s).

The total solid surface free energy and its components were determined, using distilled and deionised water and diiodomethane as testing liquids (Merk Schuchardt, $> 99\%$) doubly distilled under vacuum. This determination was based on Young's equation (2) which relates the surface tension of a liquid in equilibrium with its vapour, γ_{LV} with the contact angle of the same liquid drop on the surface of a solid, θ [17]:

$$\gamma_{SL} = \gamma_{SV} - \gamma_{LV}\cos\theta, \tag{2}$$

where γ_{SL} is the interfacial free energy between the solid and the liquid, γ_{SV} the surface free energy of the solid in equilibrium with liquid vapour, γ_{LV} the surface tension of the liquid in equilibrium with its own vapour, and θ the contact angle. The difference $\gamma_{SV} - \gamma_{SL}$ may be obtained from Eq. (2), with γ_{LV} and θ being the only parameters that can be experimentally measured.

The work of adhesion (the negative of the Gibbs energy of adhesion) for a liquid and a solid in contact, W, may be achieved using the Young–Dupré equation [18]

$$W = \gamma_{LV} + \gamma_{SV} - \gamma_{SL} = \gamma_{LV}(1 + \cos\theta). \tag{3}$$

According to Owens and Wendt [19], the solid–liquid interfacial tension can be calculated based on the assumption that the total surface free energy is expressed as a sum of two components arising from dispersive and polar contributions, γ_d and γ_p respectively. Furthermore, the work of adhesion may be treated according to the geometric mean approach [19] which implies that the solid–liquid interfacial free energy is written as

$$\gamma_{SL} = \gamma_{SV} + \gamma_{LV} - 2\sqrt{\gamma_{SV}^{d}\,\gamma_{LV}^{d}} - 2\sqrt{\gamma_{SV}^{p}\,\gamma_{LV}^{p}}. \tag{4}$$

γ_{SV} and γ_{SL} can be calculated from Eqs. (2) and (4) using experimental values of contact angles measured with a pair of testing liquids with known polar and dispersive components.

Protein studies were performed using bovine serum albumin (BSA) (Serva, ref. 11930, standard grade, lyophilised) dissolved in simulated body fluid (SBF), pH = 7.2, with the following ionic concentrations: 142.0 mM Na^+, 5 mM K^+, 2.5 mM Ca^{2+}, 1.5 mM Mg^{2+}, 4.2 mM HCO_3^{2-}, 148.0 mM Cl^-, 1.0 mM HPO_4^{2-} and 0.5 mM SO_4^{2-}. Protein adsorption studies were based on contact angle and surface tension variation with time of a 4 mg/ml albumin solution, which was prepared immediately before use. Contact angles and surface tensions were determined on six samples by the sessile and pendent drop methods, respectively.

3. Results

Results from quantitative phase analysis of HA and HA-glass composite coatings obtained by XRD patterns using the Rietveld method are shown in Table 2. The relative proportion of β-$Ca_3(PO_4)_2$ (β-TCP) in the structure of the composite coatings increased as the level of glass content added to HA increased. β-TCP was formed by the reaction of P_2O_5 glass with HA. However, HA coatings were also partially converted into β-TCP, due to phase transformations taking place during thermal cycle imposed by plasma spraying.

In Table 3 arithmetical mean roughness (R_a) values are shown. No significant differences were observed between coatings; however uncoated sand blasted Ti–6Al–4 V alloy presented a higher R_a value. Therefore, the differences in wettability and surface charge of the coatings

Table 2
Quantitative phase proportions of coatings determined by Rietveld analysis

	Quantitative phase proportions		
	HA	β-TCP	CaO
HA	87.2 ± 0.5	6.4 ± 1.3	6.4 ± 1.8
HA/$G_1$2	84.7 ± 0.9	10.9 ± 0.8	4.4 ± 0.4
HA/$G_1$4	75.3 ± 0.3	22.5 ± 3.7	2.2 ± 0.1

Table 3
Arithmetical mean roughness (R_a) for uncoated Ti–6Al–4 V, HA and composite coatings (μm)

Material	R_a
Ti–6Al–4V	6.90 ± 0.7
HA	1.37 ± 0.2
HA/$G_1$2	1.42 ± 0.2
HA/$G_1$4	1.43 ± 0.1

Table 4
Zeta potential values of HA and composite coatings powders detached from the substrate ± standard deviation (mV)

Materials	Zeta potential
HA	−9.9 ± 1.2
HA/$G_1$2	−12.5 ± 1.0
HA/$G_1$4	−14.7 ± 0.9

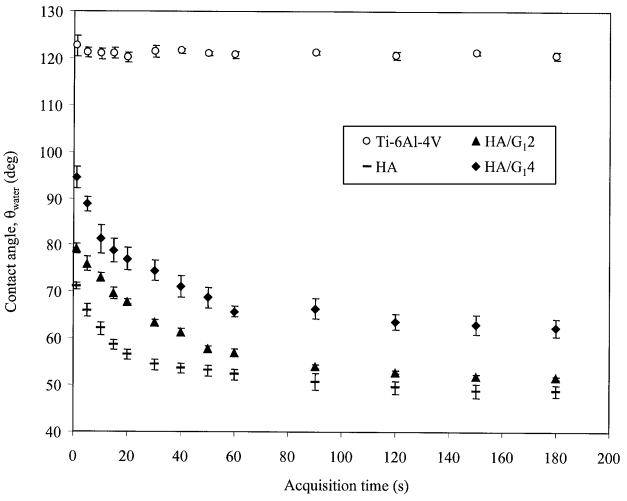

Fig. 1. Contact angle measurements for water on uncoated Ti–6Al–4 V, HA, HA/$G_1$2 and HA/$G_1$4 coatings.

Table 5
Surface free energy γ_{sv} (mJ/m^2), dispersive γ^d_{sv} and polar γ^p_{sv} components and polarity $\gamma^p_{sv}/\gamma_{sv}$ for uncoated Ti–6Al–4 V, HA, HA/$G_1$2 and HA/$G_1$4 coatings

	Ti–6Al–4V	HA	HA/$G_1$2	HA/$G_1$4
γ^d_{sv} (mJ/m^2)	35.1	26.4	21.8	23.3
γ^p_{sv} (mJ/m^2)	1.8	11.2	8.5	2.5
γ_{sv} (mJ/m^2)	36.9	37.6	30.3	25.8
Polarity	0.05	0.3	0.28	0.1

should be attributed to physico-chemical phenomena and not related to morphological surface differences.

Zeta potential of HA and composite powders are shown in Table 4. The composites presented lower values of *ZP* than HA and an increase in the percentage of β-TCP in the structure induced a more negative charged surface. This phenomenon will be discussed later. *ZP* value for titanium was not determined but literature reports $ZP = -32.6$ mV at pH = 7.15 [20].

The variation of the contact angles with acquisition time using water as testing liquid is shown in Fig. 1. After a certain acquisition period the slope of the curve decreased and the contact angle tended towards a constant value. The behaviour of Ti–6Al–4 V appears to be somehow different, with the stabilisation period being much shorter and presenting a much higher contact angle than the ceramic coatings. The water contact angle value around 121° found for the Ti–6Al–4 V alloy is higher than that reported in literature for the same alloy when polished, which should be attributed to the high surface roughness (Table 3). Concerning the coatings, the HA coating presented the lowest contact angle and HA/$G_1$4 the highest one. HA/$G_1$2 exhibited an intermediate behaviour between these materials.

The contact angles obtained using diiodomethane reached a plateau in few seconds, and remained constant, with values of 49.7 ± 1.6°, 57.4 ± 3.2°, 65.9 ± 2.9° and 66.9 ± 2.7° for Ti–6Al–4 V, HA, HA/$G_1$2 and HA/$G_1$4 respectively (data not shown).

The observed decrease of the water contact angle with time was certainly due to the absorption of the liquid drop through the microscopic pores of the coatings. In contrast, the diiodomethane molecules being larger were not able to penetrate into the pores leading to constant contact angles. All coatings presented some CaO phase although in very small contents, ranging from 2.2 to 6.4 mol%, as described in Table 2. This phase is known as being quite reactive and therefore could have also contributed to the initial time-dependent changes observed in water measurements. However, the absence of any marks on the surface after the drops having been removed rules out the possibility of any significant chemical reaction of the substrate.

As shown in Table 5 solid surface free energy varied between 37.6 and 25.8 mJ/m^2 for HA and HA/$G_1$4 respectively, while HA/$G_1$2 and the uncoated Ti–6Al–4 V

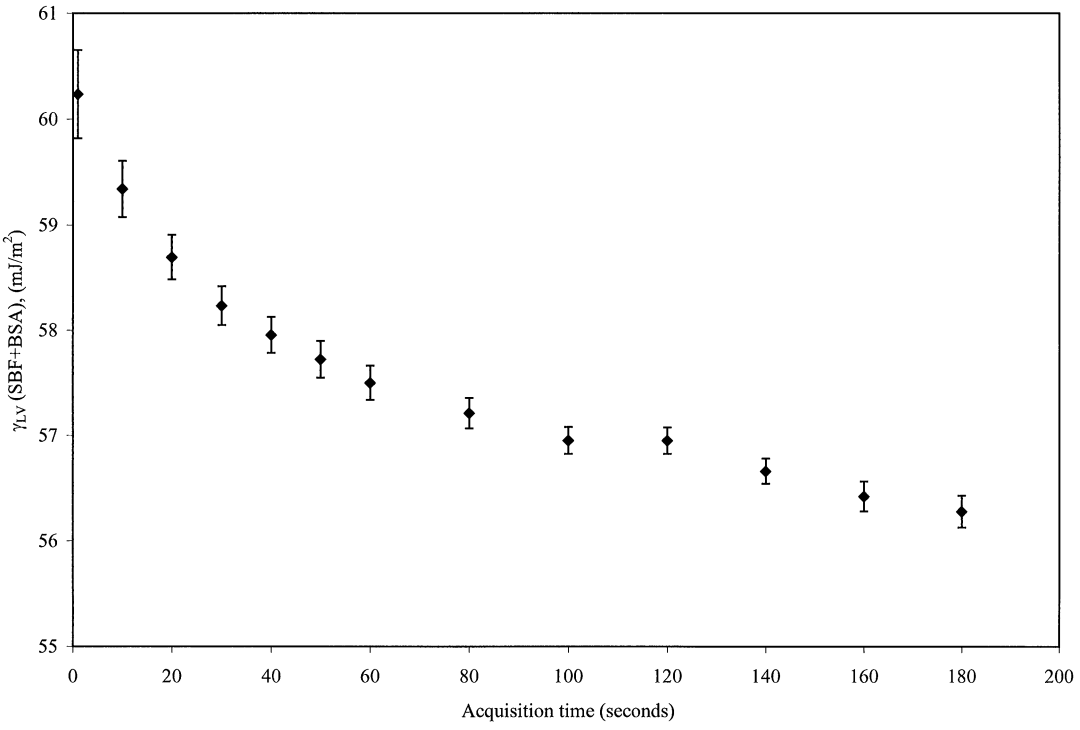

Fig. 2. Surface tension of SBF + BSA solution (in mJ/m^2) as a function of time.

presented intermediate values. In previous work [21], different values were determined on composites of similar type but samples were fully dense ceramics, which were obtained through a sintering route. Therefore, both crystallinity and morphological characteristics of these samples were different from the plasma sprayed coatings in this study.

Although the dispersive component of the surface free energy is the predominant one for all materials, the polar component gives a significant contribution, especially in the HA and HA/$G_1$2 coatings. Considering that polarity is a quantitative indicator of hydrophilicity, the uncoated Ti–6Al–4V with minimum polarity was the most hydrophobic surface. Among the coatings, the composite HA/$G_1$4 is the most hydrophobic coating. Comparison of Tables 2 and 5 shows that this coating is the one with the highest percentage of β-TCP which confirms the direct relationship between the percentage of β-TCP and the hydrophobicity of P_2O_5 glass-reinforced hydroxyapatite composites found in previous studies [21].

In Fig. 2 the evolution of the surface tension γ_{LV} of the SBF + BSA solution with time is shown. The observed decrease is typical of protein aqueous solutions [22,23] and derives from the migration and subsequent adsorption of the BSA molecules on the solution/air interface. The time dependence of the contact angles of the protein solution is shown in Fig. 3. Considering the Young–Dupré equation (3) to be valid in a dynamic situation, the time dependence of the work of adhesion,

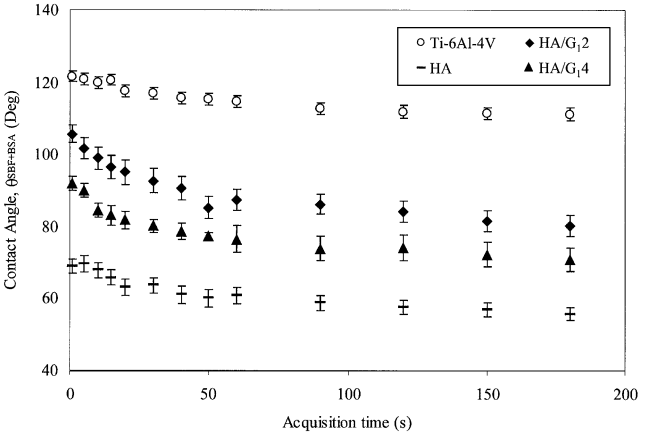

Fig. 3. Contact angle measurements for SBF + BSA on uncoated Ti–6Al–4V, HA, HA/$G_1$2 and HA/$G_1$4 coatings.

W, may be evaluated from the values of $\gamma_{LV}(t)$ and $\theta(t)$ for the albumin solution. Fig. 4 represents adhesion work for the materials under study in contact with the SBF + BSA solution. The adhesion work value found for uncoated Ti–6Al–4V was considerably lower than for the coatings. Concerning the coatings, HA was found to present the highest adhesion work with respect to the BSA solution, HA/$G_1$4 being the one with the lowest value. Once again the adhesion work value for the HA/$G_1$2 was between HA and HA/$G_1$4.

To understand the influence of the presence of the protein on the behaviour of the solid/liquid interface, we compared the work of adhesion of the aqueous solution SBF + BSA (Fig. 4) with the work of adhesion of pure water shown in Fig. 5. The analysis of both figures showed the same ordering for the work of adhesion, meaning that the addition of the protein does not change the relative surface wettability. However, for each coating the addition of protein leads to a decrease in the work of adhesion, this effect being more significant on the composites. In contrast, the presence of albumin leads to a slight increase of the work of adhesion of Ti–6Al–4 V, the most hydrophobic surface.

Finally, we should comment on the time dependence of the work of adhesion involving both water and the BSA solution. The significant increase in the work of adhesion between water and the coatings observed during the first minute of solid/liquid contact is the result of the decrease in the water contact angle. In the case of the BSA solution, the opposite effects of the decrease in the contact angle and in the surface tension upon the adhesion work (see Eq. (3)) yield much smaller variations of W.

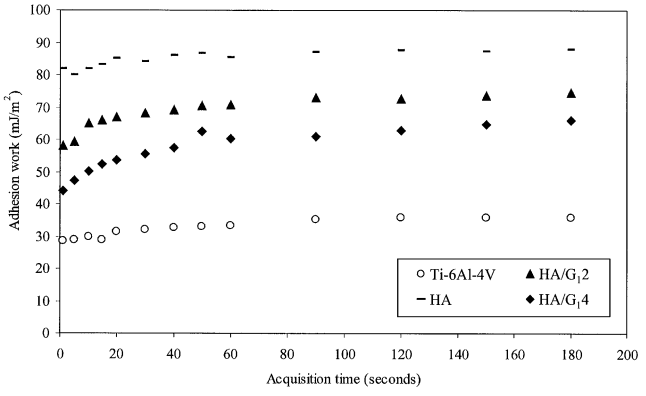

Fig. 4. Adhesion work (mJ/m^2) between SBF + BSA solution and the materials as a function of time.

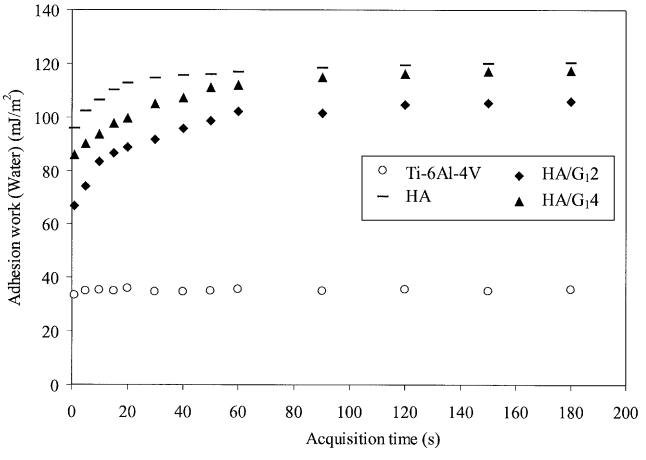

Fig. 5. Adhesion work (mJ/m^2) between water and the materials as a function of time.

4. Discussion

The interactions among biomaterials, the physiological fluids, and the host tissue after implantation are influenced by their chemistry, morphology and surface characteristics. Bioactivity and biocompatibility of these new coating materials have previously been evaluated [8,9], and relevant differences were detected between the composites. This study is a tentative attempt to elucidate the surface properties that may influence their biological behaviour.

In the plasma spraying process, the heat generated by the plasma partially decomposes the HA powder into β-TCP, which is a high temperature phase, according to the $CaO–P_2O_5$ phase diagram. This transformation leads to the liberation of OH^- groups from the $Ca_{10}(PO_4)_6(OH)_2$ structure, with production of β-TCP. Some authors have previously shown that P_2O_5 glasses react with HA powder resulting in the formation of β-TCP. Therefore, in composite coatings a higher percentage of this phase was expected than in HA coatings, due to the synergistic effect of P_2O_5 glass and the heat-induced transformation of HA.

It is presumed that cell adhesion is controlled by the mutual interactions between cells and implanted materials, such as hydrophobic bonding, hydrogen bonding and ionic affinity. Generally, in ceramics it is considered that electrostatic interaction plays an important role because of their unsatisfied oxygen ions. The surface charge of calcium phosphates has a strong effect on cell adhesion, as has recently been proved [24,25]. Therefore, it is important to analyse the actual state of the interface between the material and the solution (material surface charge, ionic concentration and polarity of the absorbed ions), with zeta potential measurements being a unique method to achieve these properties [25].

The negative values of ZP obtained for these materials are in accordance with published results for calcium phosphate ceramics. Previous works in dense ceramics have shown that for similar conditions the net negative surface charge for β-TCP is higher than for HA [21]. In the studied coatings, the percentage of β-TCP seemed to be related to the surface charge, given that the higher the percentage of β-TCP, the higher net negative surface charge for the coating.

At physiological pH both the materials under study and albumin exhibited a net negative charge [20]. More importantly, composite coatings presented a higher net negative charge than HA. Protein adsorption is a very complex process; however it is generally accepted that it is partially governed by hydrophobicity and electric surface charge [21,24,26]. Both the HA and composites

presented net negative surface charge and albumin is also negative at pH 7.2 (Table 4). Although no definite statement can be made regarding the mechanism that governed protein adsorption, it may be speculated that albumin adsorption to HA coating was somehow more effective due to its lower negative charge than that of the composite coatings. Previous studies have demonstrated that protein adsorption tends to be higher on hydrophobic materials [26], so if this phenomenon was only regulated by hydrophobicity, composite coatings would have presented higher protein adsorption than HA coating.

Although the work of adhesion, W, cannot be considered a direct measurement of protein adsorption, it quantifies the decrease in the interfacial free energy, γ_{SL} due to protein adsorption. The analysis of Figs. 4 and 5 showed that the values of the work of adhesion of both the protein solution and water are higher for HA than for the composite coatings, being minimum for Ti–6Al–4 V. For each coating the addition of protein leads to a decrease in the work of adhesion, this effect being more significant on the composites. Considering that adsorption is associated with a decrease in γ_{SL} and a concomitant increase in the work of adhesion, W (Eq. (3)), the observed decrease in the work of adhesion seems to indicate that adsorption was not significant. However, BSA is known to adsorb onto inorganic surfaces, namely HA [27]. The observed decrease in the work of adhesion should then simply mean that the protein molecules suffered structural rearrangements during adsorption. In contrast, the presence of albumin leads to the expected increase in the work of adhesion on Ti–6Al–4 V, the most hydrophobic surface [26]. This increase should result from the known tendency for the proteins to adsorb on hydrophobic surfaces.

In previous work [21], it has been observed that the work of adhesion of vitronectin solutions was higher on dense composites than on HA. However, the samples are of a different nature not only in terms of the chemical composition of the P_2O_5-glass used and surface morphology of the samples, but also due to the fact that plasma sprayed coatings are non-equilibrium materials which result from rapid cooling from the extremely high temperature of the plasma flame.

This study has clearly demonstrated that wettability and surface charge of plasma sprayed HA coatings may be changed in a controlled manner with additions of $CaO–P_2O_5$ glass, which may lead to relevant modifications in the biological behaviour of this type of biomaterials.

References

[1] Klein CPAT, Patka P, Van der Lubbe HBM. Plasma-sprayed coatings of tetracalciumphosphate, hydroxyl-apatite, and α-TCP on titanium alloy: an interface study. J Biomed Mater Res 1991;25:53–65.

[2] Jansen JA, Van der Waerden JP, Wolke JG. Histologic investigation of the biologic behavior of different hydroxyapatite plasma-sprayed coatings in rabbits. J Biomed Mater Res 1993;14:603–10.

[3] Frayssinet P, Tourenne F, Rouquet P, Conte P, Delga C, Bonel G. Comparative biological properties of HA plasma-sprayed coatings having different crystallinities. J Mater Sci: Mater Med 1994;5:11–7.

[4] Courteney-Harris RG, Kayser MV, Downes S. Comparison of the early production of extracellular matrix on dense hydroxyapatite and hydroxyapatite-coated titanium in cell and organ culture. Biomaterials 1995;16:489–95.

[5] Labat B, Chanson A, Frey J. Effects of γ-alumina and hydroxyapatite coatings on the growth and metabolism of human osteoblasts. J Biomed Mater Res 1995;29:1397–401.

[6] de Santis D, Guerriero C, Nocini PF, Ungersbock A, Richards G, Gotte P, Armato U. Adult human bone cells derived from jaw bones cultured on plasma-sprayed or polished surfaces to titanium or hydroxyapatite discs. J Mater Sci: Mater Med 1996;7:21–8.

[7] Silva PL, Santos JD, Monteiro FJ, Knowles JC. Adhesion and microstructural characterisation of plasma-sprayed hydroxyapatite/glass ceramic coatings onto Ti–6Al–4V substrates. Surf Coating Technol 1998;102:191–6.

[8] Ferraz MP, Monteiro FJ, Santos JD. $CaO–P_2O_5$ glass hydroxyapatite double-layer plasma-sprayed coating: in vitro bioactivity evaluation. J Biomed Mater Res 1999;45:376–83.

[9] Ferraz MP, Fernandes MH, Trigo Cabral A, Santos JD, Monteiro FJ. In vitro growth and differentiation of osteoblast-like human bone marrow cells on glass reinforced HA plasma-sprayed coatings. J Mater Sci: Mater Med 1999;10(9):567–76.

[10] Lapin M, Warocquier-Clérout R, Legris C, Degrange M, Luizard MFS. Correlation between roughness and wettability, cell adhesion and cell migration. J Biomed Mater Res 1997;36:99–108.

[11] Williams DF, editor. Fundamental aspects of biocompatibility. Boca Raton: CRC Press, 1982.

[12] Adamson W, editor. Physical chemistry of surfaces, 5th ed. New York: Wiley, 1990.

[13] Santos JD, Reis RL, Monteiro FJ, Knowles JC, Hastings GW. Liquid phase sintering of hydroxyapatite by phosphate and silicate glass additions: structure and properties of the composites. J Mater Sci: Mater Med 1995;6:348–52.

[14] Lopes MA, Santos JD, Monteiro FJ, Knowles JC. Glass-reinforced hydroxyapatite: a comprehensive study of the effect of glass composition on the crystallography of the composite. J Biomed Mater Res 1998;39:244–51.

[15] Chen P, Li D, Boruvka L, Rotenberg Y, Neumann AW. Automation of axisxymetric drop shape analysis for measurements of interfacial tensions and contact angles. Coll and Surf 1990;43:151–97.

[16] Cheng P, Neumann AW. Computational evaluation of axisymmetric drop shape analysis-profile (ASA-P). Coll and Surf 1992;62:297–306.

[17] Young T. In: Peacock G, editor, Miscellaneous works, vol. 1. London: Murray, 1835. p. 418.

[18] Schrader ME. Young Dupré revisited. Langmuir 1995;11:3585.

[19] Owens DK, Wendt RD. Estimation of the surface free energy of polymers. J Appl Polym Sci 1969;13:1741–69.

[20] Williams RL, Williams DF. Albumin adsorption on metal surfaces. Biomaterials 1988;9:206–12.

[21] Lopes MA, Monteiro FJ, Santos JD, Serro AP, Saramago B. Hydrophobicity, surface tension, and zeta potential measurements of glass-reinforced hydroxyapatite composites. J Biomed Mater Res 1999;45:370–5.

[22] Tripp BC, Magda JJ, Andrade JD. Adsorption of globular proteins at the air/water interface as measured via dynamic surface tension: concentration dependence, mass-transfer and adsorption kinetics. J Coll Interface Sci 1995;173:16–27.

[23] Voigt A, Thiel O, Williams D, Policova Z, Zing W, Neumann AW. Axisymmetric drop shape analysis (ADSA) applied to protein solutions. Coll and Surf 1991;58:315–26.
[24] Suzuki T, Nishizawa K, Yokogawa Y, Kameyama T. Time-dependent variation of the surface structure of bioceramics in tissue culture medium and the effect of adhesiveness of cells. J Ferment Bioeng 1996;81:226–32.
[25] Susuki T, Yamamoto T, Yoriyama M, Kameyama T. Surface instability of calcium phosphate ceramics in tissue culture medium and the effect on adhesion and growth of anchorage-dependent animal cells. J Biomed Mater Res 1997;34:504–17.
[26] Haynes CA, Norde W. Globular proteins at solid/liquid interfaces. Coll and Surf B: Biointerfaces 1994;2:517–66.
[27] Kondori K, Soito M, Takebe T, Yasukawa A. Adsorption of bovine serum albumin on synthetic carbonate calcium hydroxyapatite. J Coll Interface Sci 1995;184:124–9.